Effect of electron-electron interactions on the Klein paradox in graphene-based double-barrier structures

Chunxu Bai, Yanling Yang, and Xiangdong Zhang
Department of Physics, Beijing Normal University, Beijing 100875, China
(Received 27 June 2009; revised manuscript received 7 September 2009; published 15 December 2009)

The effects of Coulomb interactions on the transport properties of the relativistic electron through graphene-based double-barrier structures have been investigated. A self-consistent Green's function method has been developed by solving numerically the Dyson equation in the Hartree-Fock approximation. The transmission probability, conductivity, shot noise, and Fano factor through the structures have been calculated and analyzed. It is shown that Klein tunneling is suppressed strongly by taking into account the electron-electron interaction. In contrast, the Fano factor shows abrupt increase. The shot noise is either improved or suppressed, which depends on the energy of the incident electron and the strength of the electron-electron interaction. The physical originations for these phenomena have been discussed.

DOI: 10.1103/PhysRevB.80.235423 PACS number(s): 73.43.Cd, 81.05.Uw, 73.63.Bd

I. INTRODUCTION

In recent years, there has been increased interest in studying the physical properties of graphene and graphene-based microstructures since their experimental realization.[1] In graphene, the quasiparticle excitations around the Dirac point obey linear Dirac-type energy dispersion law, which can be described by a two-dimensional Dirac equation.[2,3] The presence of such Dirac-type quasiparticles is expected to lead to a number of unusual electronic properties and opens the possibility to study relativistic effects such as Klein paradox[4–12] and Zitterbewegung[13–15] in the condensed-matter experiments.

The Klein paradox describes a tunneling phenomenon of a relativistic electron through a high potential barrier.[4] It predicts that the electron can pass through the high potential barrier to approach the perfect transmission in contrast to the conventional nonrelativistic tunneling where the transmission probability exponentially decays with the increasing of the barrier height. Recently, such a phenomenon in various graphene-based microstructures such as single-barrier and double-barrier structures,[5,6] quantum well and dot,[7–9] and *n-p* junctions[10] and superlattice[11] has been investigated theoretically. The experimental observations for such a phenomenon in the graphene-based single junction have also been performed.[12] However, all these investigations neglect the effect of the electron-electron interaction.

Recent researches show that the electron-electron interaction is of crucial importance for understanding some physical properties in the graphene and graphene-based microstructures.[16–24] For example, the electron-electron interaction in suspended graphene can generate an electronic gap and result in semimetal-insulator transition,[16,17] it can provide the leading correction to the conductivity, charging accumulation, and quantum confinement effects in the microstructures.[18–24] Recent theoretical calculation of the spectral function with the electron-electron interaction enables an excellent understanding of the experimental data of angle-resolved photoemission spectroscopy.[25–28] In general, there are two kinds of method, perturbative[27–31] or nonperturbative,[16–24] to study theoretically the effect of the electron-electron interaction on physical properties in the graphene and graphene-based microstructures. For weak interactions, the perturbative approach at some cases works quantitatively well, which is in agreement with one-loop renormalization group calculations.[29,30] However, for some cases, all orders of perturbation need be considered.[31]

In this work, we investigate the effects of the electron-electron interaction on the transport properties of the relativistic electron through graphene-based double-barrier structures. We develop a self-consistent Green's function method by solving numerically the Dyson equation in the Hartree-Fock approximation. The transmission probability, conductance, shot noise, and Fano factor through the structures are calculated. The relationship between the electron-electron interaction and Klein tunneling is also analyzed in detail. The rest of the paper is organized as follows. In Sec. II, we describe the theory and method. The numerical results and discussion are presented in Sec. III. A conclusion is given in Sec. IV.

II. THEORY AND MODEL

We consider a double-barrier resonant structure $(G/IG/G/IG/G)$ in a monolayer graphene sheet occupying the xy plane, which the schematic potentials of the model are shown in Fig. 1. The left and right electrodes are separated from the central G by two barrier potential V_1 and V_2 with width d_1 and d_2, respectively. Such a local barrier can be implemented by either using the electric field effect or local chemical doping.[1,12] The potential profile $V(x)$ in the system may be adjusted independently by a gate voltage or doping, which is taken as $V(x)=V_1\Theta(x)\Theta(d_1-x)+V_2\Theta(x-L-d_1)\Theta(L+d_1+d_2-x)$. Here we assume that the electron-electron interaction bounded by the two barriers is restricted in the middle well region $(d_1<x<d_1+L)$. Meanwhile, we focus here on the case where the width (along y axis) of the graphene strip, L_y, is much larger than L. That is to say, $L\ll L_y$. In this case the details of the microscopic description of the strip edges become irrelevant. In addition, we only consider the structure without localized edge states similar to other discussions on

 ©2009 The American Physical Society

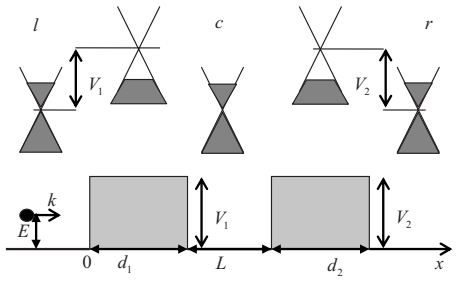

FIG. 1. Schematic diagrams of potential profile for the $G/IG/G/IG/G$ structure. The top picture corresponds to the spectrum of the quasiparticles in different monolayers. The spectrums of electron and hole are linear. The solid and dashed lines emphasize the origin of the linear spectrum, which is the crossing between the energy bands associated with crystal sublattices. The cross points represent the Dirac points. Here l, c, and r represent the region of left lead, central well, and right lead, respectively.

Klein tunneling such as Refs. 5–12. Thus, the intervalley scattering does not appear in the present case.[32]

The Hamiltonian of the system with electron-electron interaction can be written as

$$H = H_0 + H_1 \tag{1}$$

with

$$H_0 = -i\hbar v_F \sigma \nabla + V(x) \tag{2}$$

and

$$H_1 = \frac{e^2}{4\pi\varepsilon|\vec{r} - \vec{r}'|}, \tag{3}$$

where H_0 is the Hamiltonian of the system without the electron-electron interaction, $v_F \approx 10^6$ ms^{-1} is the Fermi velocity, and $\sigma=(\sigma_x,\sigma_y)$ are the Pauli matrices. Here H_1 represents the Coulomb interaction, the vectors $\vec{r}$ and $\vec{r}'$ label the positions of the electrons, and ε is the dielectric constant of the graphene. If the electron-electron interactions are neglected, the unperturbed Green's function of the system $[G^0(x,x',\varepsilon)]$ can be defined as $[\varepsilon - H_0]G^0(x,x',\varepsilon) = \delta(x-x')$, which is similar to the case of the nonrelativistic particles.[33] Such a differential equation can be solved by using the similar method in Ref. 34. Thus, the unperturbed Green's functions in different regions of the system can be obtained. According to the positions of the arguments x and x', these Green's functions can be grouped into $G^0_{cc}(x,x',\varepsilon)$, $G^0_{cl}(x,x',\varepsilon)$, $G^0_{rc}(x,x',\varepsilon)$, and $G^0_{rl}(x,x',\varepsilon)$. Suffixes denote regions in which the arguments x and x' fall. For example, $G^0_{rl}(x,x',\varepsilon)$ indicates that x is in the right region $(x > d_1+d_2+L)$ and x' in the left $(x' < 0)$. The suffix c represents the center region $(d_1 < x < d_1+L)$. If we set $d_1=d_2=d$ and $V_1=V_2=V$, these Green's functions can be expressed as

$$\begin{aligned} G^0_{cc}(x,x',\varepsilon) = {} & \frac{1}{i\hbar v_F}\begin{pmatrix} 1 & e^{-i\phi} \\ e^{i\phi} & 1 \end{pmatrix} e^{ik(x-x')} + \vartheta(e^{ik(x'-d)} r_{cl} e^{ikl} \\ & + e^{ik(L+d-x')}) r_{cr} \frac{1}{i\hbar v_F}\begin{pmatrix} 1 & -e^{i\phi} \\ -e^{-i\phi} & 1 \end{pmatrix} e^{ik(L+d-x')} \\ & + \vartheta(e^{ik(x'-d)} \\ & + e^{ik(L+d-x')} r_{cr} e^{ikL}) r_{cl} \frac{1}{i\hbar v_F}\begin{pmatrix} 1 & e^{-i\phi} \\ e^{i\phi} & 1 \end{pmatrix} e^{ik(x-d)}, \end{aligned} \tag{4}$$

$$\begin{aligned} G^0_{cl}(x,x',\varepsilon) = {} & t_{lc}\vartheta e^{ik(-x')}\left[\frac{1}{i\hbar v_F}\begin{pmatrix} 1 & e^{-i\phi} \\ e^{i\phi} & 1 \end{pmatrix} e^{ik(x-d)} \right. \\ & \left. + r_{cr}\frac{1}{i\hbar v_F}\begin{pmatrix} 1 & -e^{i\phi} \\ -e^{-i\phi} & 1 \end{pmatrix} e^{ik(2l+d-x)}\right], \end{aligned} \tag{5}$$

$$\begin{aligned} G^0_{rc}(x,x',\varepsilon) = {} & t_{cr}\vartheta e^{ik(x-L-2d)}\left[\frac{1}{i\hbar v_F}\begin{pmatrix} 1 & e^{-i\phi} \\ e^{i\phi} & 1 \end{pmatrix} e^{ik(x'-d+L)} r_{cl} \right. \\ & \left. + \frac{1}{i\hbar v_F}\begin{pmatrix} 1 & -e^{i\phi} \\ -e^{-i\phi} & 1 \end{pmatrix} e^{ik(L+d-x')}\right], \end{aligned} \tag{6}$$

$$G^0_{rl}(x,x',\varepsilon) = e^{ik(-x')} t_{lc} e^{ikL} \vartheta t_{cr} \frac{1}{i\hbar v_F}\begin{pmatrix} 1 & e^{-i\phi} \\ e^{i\phi} & 1 \end{pmatrix} e^{ik(x-L-2d)}. \tag{7}$$

Where $K=\varepsilon/\hbar v$, $k=K\cos\phi$, and ϕ is the incidence angle of the electron; $\vartheta = 1/(1-e^{2ikd} r_{cl} r_{cr})$; r_{cl} and r_{cr} represent the reflection amplitudes from the region c into regions l and r, respectively. Here t_{lc} corresponds to the transmission amplitude from the region l into the region c and t_{cr} to that from the region c into the region r. If the electron-electron interaction is considered and assumed to be restricted in the well region bounded by the two barriers, the Green's functions of the system can be obtained by a perturbation expansion in the interacting representation. Due to the translational symmetry holding for the parallel component of the wave vector, we only consider one-dimensional Green's function which propagates along the x axis. Such a Green's function in the well region is expressed by the following Dyson equation:

$$\begin{aligned} G_{cc}(x,x';\varepsilon) = {} & G^0_{cc}(x,x';\varepsilon) \\ & + \int dx_1 dx_1' G^0_{cc}(x,x_1;\varepsilon)\Sigma(x_1,x_1';\varepsilon) G_{cc}(x_1',x';\varepsilon). \end{aligned} \tag{8}$$

Here $\Sigma(x_1,x_1')$ represents the self-energy of the system. It is determined by only the Green's function G_{cc} among the four types of the self-consistent Green's functions because we have assumed that the Coulomb interaction works exclusively in the well region. In the Hartree-Fock approximation, it is described by the following form:

$$\Sigma(x_1,x_1') = 2\delta(x_1 - x_1')\int_{d_1}^{L+d_1} dx_2 V'(x_1 - x_2)\int_{-\mu_M}^{0} d\varepsilon\left(-\frac{1}{\pi}\right) \times \mathrm{Im}\, G_{cc}(x_2,x_2,\varepsilon) - V'(x_1 - x_1')\int_{-\mu_M}^{0} d\varepsilon\left(\frac{i}{2\pi}\right) \times [G_{cc}(x_1,x_1',\varepsilon) - G_{cc}^*(x_1',x_1,\varepsilon)]. \quad (9)$$

Where the function $V'(x-x')$ is the one-dimension effective Coulomb potential, which can be given by

$$V'(x-x') = \int dy dy' f_0^*(y) f_0^*(y') H_1 f_0(y') f_0(y). \quad (10)$$

Here $f_0(y) = \frac{1}{\sqrt{L_y}} \exp \frac{i}{\hbar} py$ is separable normalized wave function along y direction and p is quantized momentum. In fact, when $L \ll L_y$, it can be regarded as continue spectrum approximately. Inserting $f_0(y)$ into Eq. (10), we find that the one-dimension effective Coulomb potential is independent on the p in the calculation. The integration in Eq. (10) is taken over in the region $0 < y < L_y$.

Noting that the self-energy Σ in Eq. (9) also contains the Green's function G_{cc}, so we have to solve Eqs. (8) and (9) self-consistently. In order to solve numerically these integral equations, we need discretize the continuous coordinate and energy. The coordinate x within the well region is divided into N_x elements, the energy between 0 and μ_M is divided into N_y regions. The values of the N_x and N_y determine the accuracy of the calculation. We can obtain the solutions with high accuracy through choosing suitable N_x and N_y.

After the Green's function G_{cc} is obtained, the other Green's functions such as G_{cl} and G_{rl} can be obtained by the following Dyson equation:

$$G_{cl}(x,x';\varepsilon) = G_{cl}^0(x,x';\varepsilon) + \int dx_1 dx_1' G_{cc}^0(x,x_1;\varepsilon)\Sigma(x_1,x_1';\varepsilon)G_{cl}(x_1',x';\varepsilon) \quad (11)$$

and

$$G_{rl}(x,x';\varepsilon) = G_{rl}^0(x,x';\varepsilon) + \int dx_1 dx_1' G_{rc}^0(x,x_1;\varepsilon)\Sigma(x_1,x_1';\varepsilon)G_{cl}(x_1',x';\varepsilon). \quad (12)$$

Then, the transmission amplitude t_{total} through the double-barrier structure can be calculated by the following equation:

$$t_{total}(E) = i\hbar v_F G_{rl}(L + d_1 + d_2, 0). \quad (13)$$

Therefore, the tunneling probability is given by $T = |t_{total}(E)|^2$.

After the transmission coefficients are obtained, the total conductivity can be calculated. According to Buttiker formula,[11] at zero temperature the total conductivity in this system is given by

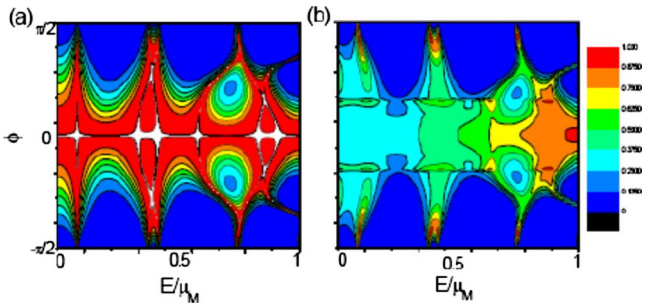

FIG. 2. (Color online) Transmission probability (T) as a function of the angle (ϕ) and the energy (E) of the incident electron. (a) and (b) correspond to the case without ($\mu/\mu_M = 0$) and with ($\mu/\mu_M = 0.4$) the electron-electron interaction, respectively. Here $L = 50$ nm, $d = 50$ nm, $L_y = 500$ nm, $V = 200$ meV, and $\mu_M = 80$ meV.

$$G = G_0 \int_0^{\pi/2} T(E, \sqrt{2E}\sin\phi)\cos\phi d\phi, \quad (14)$$

where $G_0 = 2e^2 m v_F L_y/\hbar^2$, L_y is the width of the graphene strip (along y axis). Similarly, we can also study the shot noise (S) and Fano parameter (F) in the system[35,36]

$$S = S_0 \int_0^{\pi/2} T(1-T)\cos\phi d\phi, \quad (15)$$

$$F = \frac{\int_{-\pi/2}^{\pi/2} T(1-T)\cos\phi d\phi}{\int_{-\pi/2}^{\pi/2} T\cos\phi d\phi}, \quad (16)$$

where $S_0 = 16\frac{e^3 V}{h}\frac{EL_y}{\pi\hbar v_F}$, E is the energy of the incident electron. Combining Eqs. (13)–(16), the conductivity, shot noise, and Fano parameter for the double-barrier structures can be obtained by the numerical calculations.

III. NUMERICAL RESULTS AND DISCUSSION

In this section, we provide comparison between the numerical results in the presence and absence of the electron-electron interaction. The calculated results for the transmission probability T as a function of the angle (ϕ) and the energy (E) of the incident electron are plotted in Fig. 2. Here the thicknesses of the well and the barrier are taken as $L = 50$ nm and $d = 50$ nm, respectively. The transverse width of the graphene strip is taken as $L_y = 500$ nm. The strength of the barrier is taken as $V = 200$ meV and the maximal chemical potential in the well region is taken as $\mu_M = 80$ meV.[5,14] Figure 2(a) shows the calculated results without the electron-electron interactions and Fig. 2(b) corresponds to that with the electron-electron interaction ($\mu/\mu_M = 0.4$). In the calculation we find that the sum of the transmission and reflection coefficients is near 1 and the error is controlled below 1%, when the discrete elements N_x and N_y are taken as 20 and 200, respectively. It is seen from Fig. 2(a) that the structure remains always perfectly transparent for the normal incidence, no matter what the value of the energy for the incident

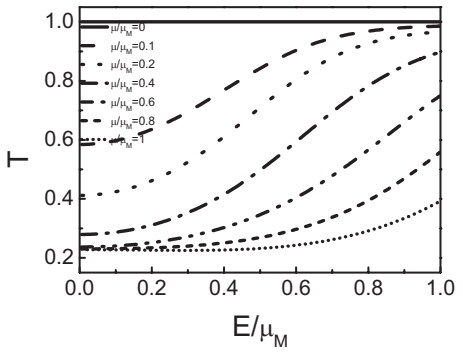

FIG. 3. Transmission probability (T) of the normal incident electron as a function of E with various chemical potential in the quantum well. Solid line, dashed line, dotted line, and dot-dashed line correspond to $\mu/\mu_M=0$, $\mu/\mu_M=0.2$, $\mu/\mu_M=0.6$, and $\mu/\mu_M=1$, respectively. The other parameters are taken the same as in Fig. 2.

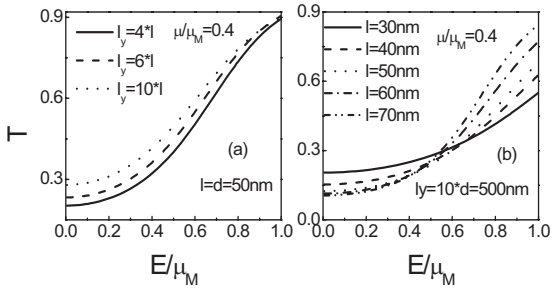

FIG. 4. (a) Transmission probability (T) of the normal incident electron as a function of E with various well width and (b) transverse width of the sample. The other parameters are marked in the figures.

electron is. This is the feature unique to massless Dirac fermions and directly related to the Klein tunneling. Due to the chiral nature of the quasiparticles, the tunneling is also highly anisotropic and the angular dependence of transmission probability exhibits oscillation behavior, which has been pointed out in previous investigation.[11]

However, the changes take place with the introduction of the electron-electron interaction. It is seen from Fig. 2(b) that the peak of the transmission probability shifts toward higher energy, although the oscillation phenomena still keep. This is because the Coulomb energy appears after the electron-electron interaction is taken into account, which results in the change in the chemical potential in the well. The other striking feature is that the transmission probability is suppressed strongly. This can be seen more clearly from Fig. 3.

Figure 3 shows the transmission probabilities of the normal incident electron as a function of incident energy with various chemical potential in the well. Increasing the value of the chemical potential, corresponding to increasing the number of electrons, makes the Coulomb energy in the well region become larger. Therefore, the strength of the electron-electron interaction is depicted by the value of the chemical potential. The solid line, dashed line, dotted line, and dot-dashed line correspond to $\mu/\mu_M=0$, $\mu/\mu_M=0.2$, $\mu/\mu_M=0.6$, and $\mu/\mu_M=1$, respectively. As can be seen clearly, the transmission probability decreases quickly with the increase in the chemical potential. For example, the transmission probability decreases 40% when $\mu/\mu_M=0.1$ is taken. It becomes 76% corresponding to $\mu/\mu_M=0.6$. In fact, such a phenomenon corresponds to the Coulomb blockade effect or the energy gap arises from the electron-electron interaction. Recently, based on the Monte Carlo method, Drut and Lähde have investigated the phase diagram of graphene material and pointed out that the electron-electron interaction can generate the energy gap in suspended graphene samples.[16] Our present results can be regarded as the corresponding to the phenomenon in the double-barrier structure.

Such a phenomenon is not sensitive to the structural parameters of the system. Figure 4(a) shows the transmission probability of the normal incident electron as a function of E with various transverse width of the sample. The solid line, dashed line, and dotted line correspond to the cases with $L_y=4L$, $L_y=6L$, and $L_y=10L$, respectively. Although the suppression of T becomes stronger with the decrease in the transverse width of the sample, the change feature keeps the same for them. For a large transverse width such as $L_y>10L$, such a size effect is negligible. The corresponding results for the transmission probability as a function of E with different well width at $L_y=10L$ are plotted in Fig. 4(b). The suppression phenomena are observed again for all cases. It is interesting that two different energy regions appear, one is at $E/\mu_M>0.55$ where the T increases with the increase in the well width and the other is at $E/\mu_M<0.55$ where the T decreases with the increase in the well width. As E/μ_M is taken around 0.55, the transmission probability is independent on the well width. This is because the strength of the electron-electron interaction increases with the decrease in the well width. At the same time, the effect of the electron-electron interaction on the transmission property decreases due to the decrease in the well width. That is to say, the above phenomena originate from the competition between the size effect and the electron-electron interaction.

With the transmission probability obtained, we now turn to the angularly averaged conductivity and shot noise properties. In Figs. 5(a) and 5(b), we plot the two-dimensional conductivity G and shot noise S through $G/IG/G/IG/G$ structure as a function of the energy of the incident electron, respectively. The solid lines, dashed lines, and dotted lines correspond to the cases with $\mu/\mu_M=0$, 0.4, and 1.0, respectively. In the absence of the electron-electron interaction, the conductivity exhibits oscillatory behaviors with the increase in the energy of the incident electron, which agrees well with those in the previous investigation.[11] With the introduction of the electron-electron interaction, the suppression effect of the conductivity is observed. For example, the conductivity is suppressed 55% at $E/\mu_M=0.6$ for $\mu/\mu_M=0.4$, the corresponding suppression can reach 86% for $\mu/\mu_M=1.0$. These are similar to the case of the transmission probability and can be understood by the same way.

In contrast, the shot noise exhibits more complex feature. First, the shot noise is also an oscillation function of the energy of the incident electron. However, the peaks of the oscillation move toward lower energy with the introduction of the electron-electron interaction, which is opposite to the

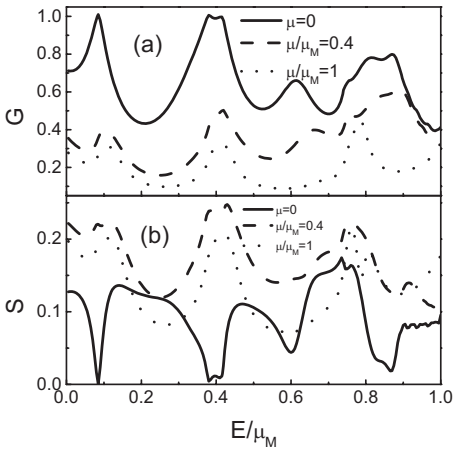

FIG. 5. (a) Conductivity and (b) shot noise as a function of E with various μ. Solid line, dashed line, and dotted line correspond to $\mu/\mu_M=0$, $\mu/\mu_M=0.4$, and $\mu/\mu_M=1$, respectively. The other parameters are taken the same as in Fig. 2.

feature of the transmission probability and the conductivity. The value of the shot noise is either improved or suppressed, which depend on the incident energy and the strength of the electron-electron interaction. As the electron-electron interaction is small, the shot noise is always improved by the effect of the electron-electron interaction. When the strength of the electron-electron interaction becomes very strong such as $\mu/\mu_M=1$ [dotted line in Fig. 5(b)], the shot noise is suppressed at some regions of the incident energy. This can be understood by the definition of the shot noise. From Eq. (15), we know that the maximum of the shot noise appears at $T=1/2$. Due to the suppression of the Klein tunneling by the electron-electron interaction, the transmission probability becomes near $T=1/2$ with the introduction of the electron-electron interaction, which leads to the increase in the S. However, when the electron-electron interaction becomes very strong, the transmission probability and conductivity are suppressed so strong that they are far lower than 1/2. This makes the shot noise becomes small in comparison with the case without the electron-electron interaction.

Another remarkable transport property in graphene microstructure is demonstrated in the Fano factor. The calculated results for the Fano factor as a function of the energy in the presence and absence of the electron-electron interaction are plotted in Fig. 6. The solid line and dashed line correspond to $\mu/\mu_M=0.4$ and $\mu/\mu_M=0$, respectively. In the absence of the electron-electron interaction, oscillations of the Fano factor with maximums $F=1/3$ are observed due to the angular anisotropy in the transmission of relativistic quasiparticles, which is agreement with the previous investigations.[35,36] When the electron-electron interaction is taken into account,

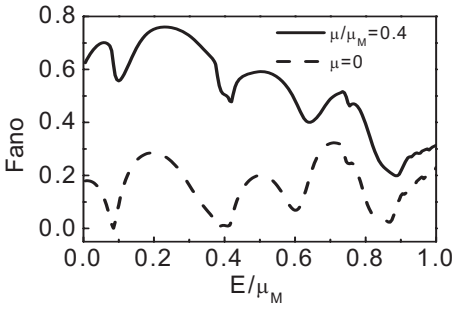

FIG. 6. Fano factor as a function of E. Solid line and dashed line correspond to $\mu/\mu_M=0.4$ and $\mu/\mu_M=0$, respectively. The other parameters are taken the same as in Fig. 2.

the Fano factor is improved largely. For example, the peaks rise from 1/3 about 0.76 and 0.85 for $\mu/\mu_M=0.4$ and $\mu/\mu_M=1.0$, respectively. The enhancement of the Fano factor can also be understood by the transmission suppression caused by the electron-electron interaction. Such a phenomenon is similar to the case of the graphene with the energy gap.

IV. SUMMARY

In the Hartree-Fock approximation, we have investigated the transport properties of the relativistic electron through the graphene-based double-barrier structures by solving the Dyson equation self-consistently. The relationship between Klein tunneling and the electron-electron interaction has been analyzed in detail. The transmission probability, conductivity, shot noise, and Fano factor have been calculated. When the electron-electron interaction is taken into account, we have found that the peak of the transmission probability not only shifts toward higher energy, its value can be suppressed strongly. When the interaction becomes larger, the conductivity can be suppressed more than 80%. This is corresponded to the Coulomb blockade effect or the energy gap arises from the electron-electron interaction. In contrast, the Fano factor shows abrupt increase. The shot noise is either improved or suppressed, which depends on the energy of the incident electron and the strength of the electron-electron interaction. We hope that our theoretical results can provide important reference to design the electron device based on the graphene materials.

ACKNOWLEDGMENTS

This work was supported by the National Natural Science Foundation of China (Grants No. 10674017 and No. 10825416) and the National Key Basic Research Special Foundation of China under Grant No. 2007CB613205.

[1] K. S. Novoselov, A. K. Geim, S. V. Morozov, D. Jiang, Y. Zhang, S. V. Dubonos, I. V. Grigorieva, and A. A. Firsov, Science **306**, 666 (2004).
[2] C. W. J. Beenakker, Rev. Mod. Phys. **80**, 1337 (2008).
[3] A. H. Castro Neto, F. Guinea, N. M. R. Peres, K. S. Novoselov, and A. K. Geim, Rev. Mod. Phys. **81**, 109 (2009).
[4] O. Klein, Z. Phys. **53**, 157 (1929).
[5] M. I. Katsnelson, K. S. Novoselov, and A. K. Geim, Nat. Phys. **2**, 620 (2006).
[6] J. M. Pereira, P. Vasilopoulos, and F. M. Peeters, Appl. Phys. Lett. **90**, 132122 (2007).
[7] K. Wakabayashi, Y. Takane, and M. Sigrist, Phys. Rev. Lett. **99**, 036601 (2007).
[8] M. I. Katsnelson, Eur. Phys. J. B **51**, 157 (2006).
[9] P. G. Silvestrov and K. B. Efetov, Phys. Rev. Lett. **98**, 016802 (2007).
[10] V. V. Cheianov and V. I. Falko, Phys. Rev. B **74**, 041403(R) (2006).
[11] C. Bai and X. Zhang, Phys. Rev. B **76**, 075430 (2007).
[12] A. F. Young and P. Kim, Nat. Phys. **5**, 222 (2009).
[13] E. Schrödinger, Sitzungsber. Preuss. Akad. Wiss., Phys. Math. Kl. **24**, 418 (1930).
[14] W. Zawadzki, Phys. Rev. B **72**, 085217 (2005); T. M. Rusin and W. Zawadzki, J. Phys.: Conf. Ser. **19**, 136219 (2007).
[15] X. Zhang, Phys. Rev. Lett. **100**, 113903 (2008); X. Zhang and Z. Y. Liu, *ibid.* **101**, 264303 (2008).
[16] Joaquín E. Drut and Timo A. Lähde, Phys. Rev. Lett. **102**, 026802 (2009); Phys. Rev. B **79**, 165425 (2009).
[17] I. F. Herbut, Phys. Rev. Lett. **97**, 146401 (2006).
[18] E. G. Mishchenko, Phys. Rev. Lett. **98**, 216801 (2007).
[19] A. K. Geim and K. S. Novoselov, Nature Mater. **6**, 183 (2007).
[20] J. S. Bunch, Y. Yaish, M. Brink, K. Bolotin, and P. L. McEuen, Nano Lett. **5**, 287 (2005).
[21] F. Sols, F. Guinea, and A. H. Castro Neto, Phys. Rev. Lett. **99**, 166803 (2007).
[22] M. Ezawa, Phys. Rev. B **77**, 155411 (2008).
[23] I. F. Herbut, V. Juricic, and O. Vafek, Phys. Rev. Lett. **100**, 046403 (2008).
[24] M. Zarea and N. Sandler, Phys. Rev. Lett. **99**, 256804 (2007).
[25] A. Bostwick, T. Ohtai, T. Seyller, K. Horn, and E. Rotenbergi, Nat. Phys. **3**, 36 (2007); New J. Phys. **9**, 385 (2007).
[26] S. Y. Zhou, G.-H. Gweoni, A. V. Fedorov, P. N. First, W. A. Deheer, D.-H. Leei, F. Guinea, A. H. Castro Neto, and A. Lanzara, Nature Mater. **6**, 770 (2007).
[27] E. H. Hwang and S. Das Sarma, Phys. Rev. B **77**, 081412(R) (2008).
[28] M. Polini, R. Asgari, G. Borghi, Y. Barlas, T. Pereg-Barnea, and A. H. MacDonald, Phys. Rev. B **77**, 081411(R) (2008).
[29] V. N. Kotov, V. M. Pereira, and B. Uchoa, Phys. Rev. B **78**, 075433 (2008).
[30] R. Roldán, M. P. López-Sancho, and F. Guinea, Phys. Rev. B **77**, 115410 (2008).
[31] V. N. Kotov, B. Uchoa, and A. H. Castro Neto, Phys. Rev. B **78**, 035119 (2008).
[32] A. R. Akhmerov, J. H. Bardarson, A. Rycerz, and C. W. J. Beenakker, Phys. Rev. B **77**, 205416 (2008).
[33] E. N. Economou, *Green's Function in Quantum Physics* (Springer-Verlag, Berlin, 1979).
[34] T. Gruner and D.-G. Welsch, Phys. Rev. A **54**, 1661 (1996).
[35] J. Tworzydło, B. Trauzettel, M. Titov, A. Rycerz, and C. W. J. Beenakker, Phys. Rev. Lett. **96**, 246802 (2006).
[36] R. Zhu and Y. Guo, Appl. Phys. Lett. **91**, 252113 (2007).